Distinct mechanisms underlie H_2O_2 sensing in *C. elegans* head and tail

Sophie Quintin[1234]*, Théo Aspert[1234], Tao Ye[1234] and Gilles Charvin[1234]
*** corresponding author (quintin@igbmc.fr)**

1) Department of Developmental Biology and Stem Cells, Institut de Génétique et de Biologie Moléculaire et Cellulaire, Illkirch, France

2) Centre National de la Recherche Scientifique, UMR7104, Illkirch, France

3) Institut National de la Santé et de la Recherche Médicale, U964, Illkirch, France

4) Université de Strasbourg, Illkirch, France

Abstract

Environmental oxidative stress threatens cellular integrity and should therefore be avoided by living organisms. Yet, relatively little is known about environmental oxidative stress perception. Here, using microfluidics, we showed that like I2 pharyngeal neurons, the tail phasmid PHA neurons function as oxidative stress sensing neurons in *C. elegans*, but display different responses to H_2O_2 and light. We uncovered that different but related receptors, GUR-3 and LITE-1, mediate H_2O_2 signaling in I2 and PHA neurons. Still, the peroxiredoxin PRDX-2 is essential for both, and might promote H_2O_2-mediated receptor activation. Our work demonstrates that *C. elegans* can sense a broad range of oxidative stressors using partially distinct H_2O_2 signaling pathways in head and tail sensillae, and paves the way for further understanding of how the integration of these inputs translates into the appropriate behavior.

Graphical abstract

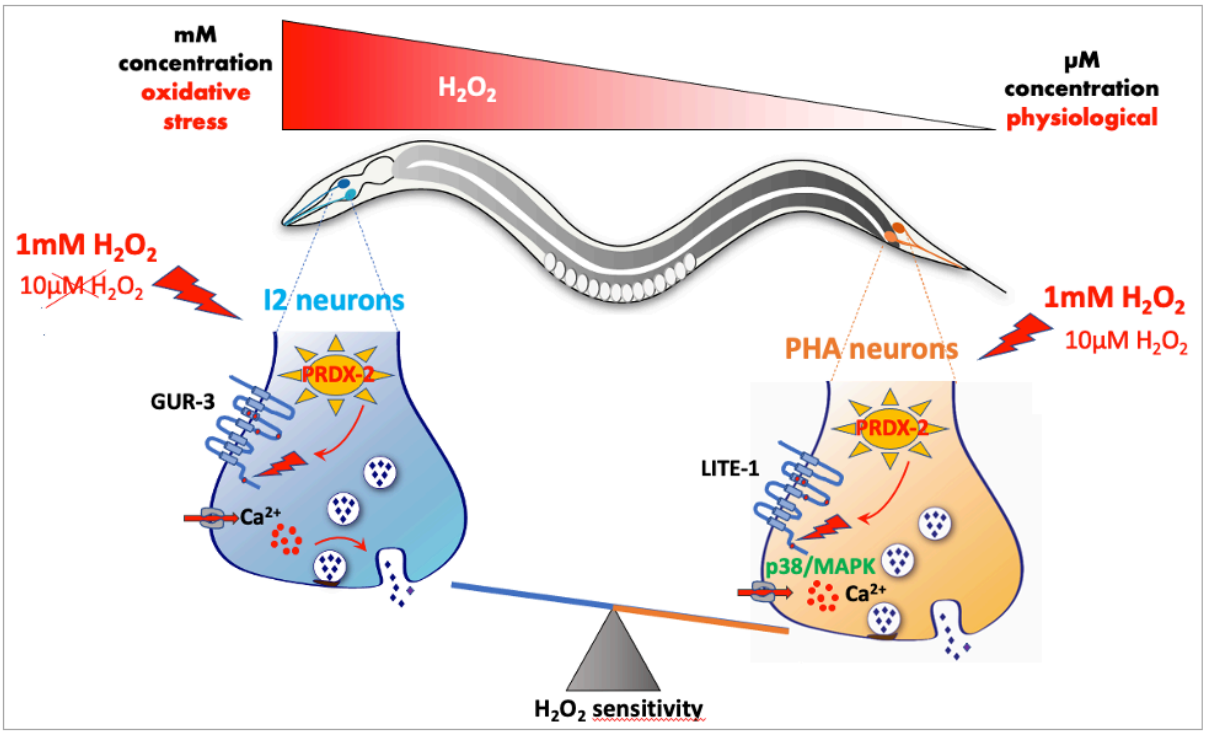

Introduction

Reactive oxygen species (ROS) are well-known to exert a dual effect, promoting aging and pathological conditions on the one hand and increasing organism resistance and longevity on the other hand (Davalli et al., 2016). Neurons are easily exposed to ROS, and many neurodegenerative diseases have been associated with oxidative stress (Cobb and Cole, 2015). However, exposure of *C. elegans* nematodes to a mild oxidative stress has been reported to be beneficial for neuron sensory function: micromolar doses of the ROS-inducing agent paraquat or of hydrogen peroxide (H_2O_2) improve the sensitivity in ASH polymodal neurons (Gourgou and Chronis, 2016; Li et al., 2016), whereas millimolar doses of H_2O_2 reduce neuron response (Li et al., 2016), likely inducing oxidative stress. Therefore, it is essential for nematodes to detect a broad range of H_2O_2 concentrations to preserve their cellular integrity.

Although the cellular response to oxidative stress has been extensively characterized (reviewed in (Blackwell et al., 2015), little is known on how oxidants are actually perceived and which underlying molecular pathways are involved. Recent studies indicate that light and H_2O_2 sensing are tightly connected in yeast (Bodvard et al., 2017) and in nematodes (Bhatla and Horvitz, 2015). While it has been demonstrated that light is converted into an H_2O_2 signal in yeast (Bodvard et al., 2017), this question remains unanswered in nematodes. Notably, *C. elegans* can detect both H_2O_2 and light via the I2 pharyngeal neurons and responds to these stimuli by inhibition of feeding or by an avoidance behavior (Bhatla and Horvitz, 2015). Initially described as interneurons, the I2 neurons proved to be primary sensory neurons exposed to the environment, and were shown to be highly specialized in oxidative stress sensing (Bhatla and Horvitz, 2015), and were recently shown to respond moderatly to salt or odor (Yemini et al., 2021)**.** However, although detection of a large spectrum of H_2O_2 is critical for nematodes, the range of H_2O_2 concentrations detected by I2 neurons has not been investigated, and the molecular mechanisms involved in H_2O_2 signaling are not well defined.

In addition, the nematode also possesses tail sensory neurons specialized in chemo-repulsion, called phasmids (PHAs and PHBs) (reviewed in (Goodman and Sengupta, 2019). In contrast to I2 neurons, these tail neurons can respond to many noxious stimuli (Zou et al., 2017) and trigger avoidance (Hilliard et al., 2002)**,** but whether PHA neurons can sense H_2O_2 or light remains an open question.

H_2O_2 sensing in I2 neurons requires the function of the peroxiredoxin PRDX-2 (Bhatla and Horvitz 2015), a highly conserved antioxidant enzyme whose role remains unclear. Peroxiredoxins (Prxs) belong to a family of thiol peroxidases which can reduce H_2O_2 in cells following the oxidation of one or two cysteines in their catalytic domain, and they are highly abundant from yeast (Breker et al., 2013; Ho et al., 2018) to human cells, in which they represent approximately 1% of the total dry cellular mass (Chae et al., 1999; Low et al., 2007). Oxidised Prxs are recycled in the reduced, active form, by thioredoxin (Hall et al., 2009). At high H_2O_2 concentrations, Prxs become hyperoxidized, a form that has been shown to function as a molecular chaperone (Jang et al., 2004; Moon et al., 2005). Similarly, thioredoxins have been shown to have redox-independent function (McCallum et al., 2016; Sanzo-Machuca et al., 2019)**.** As pivotal antioxidants, Prxs dysfunction has been associated with several pathologies (Park et al., 2016), including cancer (Ding et al., 2017). In budding yeast, the

peroxiredoxin Tsa1 has a major role in maintaining the redox balance, and is massively induced upon oxidative stress as a direct target of the H_2O_2-sensing transcription factor Yap1 (Goulev et al., 2017; Lee et al., 1999). In *C. elegans*, among three genes encoding peroxiredoxins, PRDX-2 is the only one whose depletion induces a phenotype and is considered as the major peroxiredoxin (Isermann et al., 2004; Oláhová et al., 2008). PRDX-2 is expressed in many cell types including neurons, gut (Hirani et al., 2013; Isermann et al., 2004; Oláhová et al., 2008), muscle and epithelial cells (Bhatla and Horvitz, 2015). Although a global induction of *prdx-2* mRNA expression has been reported upon treatment with the strong tBOOH oxidant (Isermann et al., 2004), cells in which PRDX-2 expression is induced remain to be identified. Likewise, the question of a tissue-specific regulation of PRDX-2 by SKN-1, the closest ortholog of Yap1, has not been addressed.

Importantly, beyond their peroxidase activity, Prxs have long been proposed to act as intracellular H_2O_2 sensors, which influence cellular signaling (Ledgerwood et al., 2017; Rhee and Woo, 2011; Veal et al., 2007). For example, the p38/MAPK signaling pathway, which controls adaptive mechanisms and/or cell fate decisions, is activated by H_2O_2 through Prxs in an evolutionary conserved manner (Barata and Dick, 2020; Jarvis et al., 2012). Like in mammalian or in drosophila cells, several studies in *C. elegans* indicate that PRDX-2 would relay H_2O_2 signaling, activating the downstream p38/PMK-1 pathway (Gomes et al., 2016; Haes et al., 2014; Li et al., 2016). Notably, low doses of H_2O_2 potentiate the sensory response of ASH sensory neurons to glycerol through activation of the PRDX-2/p38/PMK-1 cascade (Li et al., 2016). Yet, whether this cascade is at play in I2 neurons to influence H_2O_2 perception has not been analyzed.

Here, we undertook a subcellular analysis of the peroxiredoxin PRDX-2 in *C. elegans*, focusing on its requirement in neuronal H_2O_2 sensing. Using a CRISPR knock-in line, we showed that PRDX-2 is present in many cells, among which several pairs of neurons: I2s in the head, PHAs in the tail and CANs in the body. Interestingly, upon an H_2O_2 challenge, an upregulation of PRDX-2 is observed only in the anterior gut and in the excretory pore, but not in neurons, suggesting that PRDX-2 might fulfill different functions, depending on the cell type where it is expressed. Using a microfluidic-based approach and real-time calcium imaging, we show that PHA neurons also respond to H_2O_2, with an even higher sensitivity than I2 neurons. Although H_2O_2 perception depends on *prdx-2* function in both pairs of neurons, we uncovered that it relies on different gustatory receptors and downstream transducers: while dispensable in I2 neurons, the p38/MAPK kinase contributes to the hypersensitivity of PHA neurons to H_2O_2. Interestingly, we uncovered that H_2O_2 sensing requires the same receptors as light sensing, and that PHA neurons respond to light —establishing a parallel between PHA and photosensory ASH neurons. Based on our work and on previous studies, we propose a molecular model of how H_2O_2 could trigger neuronal activation in I2 and PHA through a peroxiredoxin-mediated redox relay. Taken together, our data suggest that *C. elegans* can sense a broad range of oxidative stress using partially distinct H_2O_2 signaling pathways acting in head and tail sensillae.

Results

Expression pattern of prdx-2 and its evolution upon H_2O_2 treatment

In budding yeast, the peroxiredoxin Tsa1 is massively induced upon H_2O_2 treatment (Goulev et al., 2017; Lee et al., 1999). To gain insight into the tissue-specific expression of PRDX-2 upon oxidative stress, we first used the PRDX-2 reporter line generated by (Hirani et al., 2013). However, the level of expression of this strain varies a lot, and transgenics show many fluorescent aggregates (Hirani et al, 2013; sup. Fig. 1), likely associated with transgene overexpression. Consistently, the strain displays a much stronger resistance to oxidative stress than wild-type animals (sup. Fig. 1), suggesting that overexpressed PRDX-2 construct induces a higher H_2O_2 scavengeing capacity in transgenics. Furthermore, it was impossible to identify PRDX-2-expressing cells in this strain, preventing the use of this strain in our study. For these reasons, we created a GFP knock-in line of PRDX-2, using the CRISPR-Cas9 technique (Dickinson et al., 2013). A C-terminus GFP fusion targeting all PRDX-2 isoforms, comprising a linker, was engineered and inserted at the *prdx-2* locus (Fig. 1A). Three independent knock-in lines were obtained, sharing an identical expression pattern (Fig. 1B).

In the PRDX-2::GFP knock-in line, we detected a broad expression of PRDX-2 in various cell types, including the proximal and distal gut, muscles (body wall, vulval and pharyngeal), epithelial cells (vulva, nose tip, hypodermis) and I2 neurons (Fig. 1B), consistent with previous reports (Bhatla and Horvitz, 2015; Isermann et al., 2004; Oláhová et al., 2008). In addition, we observed for the first time PRDX-2 expression in the excretory pore cell (EPC), and in two other pairs of neurons; the tail phasmids (PHA/PHB) and the excretory canal-associated neurons (CANs), located close to the vulva (Fig. 1B). Consistent with this, a high number of *prdx-2* transcripts was detected in CANs and in the EPC (Cao et al., 2017). Therefore, we hypothesized that the knock-in line faithfully reflects the endogenous PRDX-2 expression, and characterized it further.

PRDX-2 expression is induced in the anterior gut upon H_2O_2 treatment, but not in I2 neurons

We noticed that many PRDX-2-expressing cells are directly in contact with the environment, such as the EPC, the tip of the nose, the vulva, and neurons, which all possess terminations exposed outside. This pattern is strikingly reminiscent of that detected in animals carrying the *HyPer* H_2O_2 biosensor after H_2O_2 exposure (Back et al., 2012). Thus, PRDX-2 is expressed in cells in which environmental H_2O_2 penetrates more easily, suggesting a protective role of PRDX-2 in these cells as a peroxidase. Therefore, in the following, we wondered whether all PRDX-2-expressing cells respond similarly to H_2O_2-induced oxidative stress.

To determine whether PRDX-2 expression changes upon oxidative stress, we exposed animals to different doses of H_2O_2, and PRDX-2::GFP expression was quantified in different cells after spinning-disc confocal acquisitions. A higher PRDX-2 expression was detected in the anterior gut two hours after a 10mM H_2O_2 treatment, but not after a 1mM H_2O_2 treatment (Fig. 1C,E). The higher fluorescence was due to PRDX-2::GFP as H_2O_2-treated controls did not show a higher gut autofluoresecence (sup. Fig. 2). Similarly, PRDX-2 expression was only induced in the EPC at the high dose of 10mM H_2O_2 (Fig. 1F, sup. Fig. 2). Thus, our data indicate

a dose-dependent PRDX-2 induction —as it occurs at 10mM but not at 1mM. The origin of this difference could arise from the animal behavioral response: at 1mM H_2O_2 the pharyngeal pumping is strongly inhibited to prevent ingestion (Bhatla and Horvitz, 2015), thereby exposure of gut cells to H_2O_2. This could explain the absence of PRDX-2 induction at 1mM in the gut and the unchanged level of *prdx-2* mRNA reported by Isermann et al. (2004) after 1mM H_2O_2 treatment. In contrast, at 10mM H_2O_2, the nematode should retract back (avoidance response, Bhatla and Horvitz 2015); but here, as animals are trapped in wells and cannot escape, they likely swallow a certain amount of H_2O_2, exposing the foregut to a severe oxidative stress that could in turn trigger PRDX-2 induction. A 10mM H_2O_2 treatment of 30min has been shown to induce hyperoxidation of over 50% total PRDX-2 in wild-type lysed worms (Thamsen et al., 2011) and this form persists after a 4h recovery period (Oláhová et al., 2008). Still, the induction we observed suggests that PRDX-2 could scavenge H_2O_2 in the EPC and in the foregut, to exert a protective role.

Among PRDX-2-expressing neurons, the I2 pair shows the highest expression and possesses terminations exposed to the outside (Bhatla et al., 2015). Therefore, we focused on I2 neurons to investigate whether the neuronal level of PRDX-2 is affected upon H_2O_2 treatment. However, at both concentrations tested (1 and 10mM), the level of PRDX-2 in I2 neurons constantly remained unchanged after H_2O_2 treatment (Fig. 1D,F, sup. Fig. 2).

Thus, we observed an upregulation in the anterior gut and in the EPC following an acute oxidative stress, but not in neurons. As Prxs belong to a homeostatic system, an upregulation was shown to be associated with a detoxification function (Goulev et al., 2007). Therefore, these data suggest that PRDX-2 might fulfill a peroxidase function in the foregut and in the EPC to protect the animal against environmental aggressions, consistent with the reported protective role of intestinal PRDX-2 (Oláhová et al., 2008). In contrast, no upregulation of PRDX-2 has been observed in I2 neurons upon oxidative stress, suggesting that PRDX-2 would instead act in H_2O_2 sensing and/or signaling, as proposed (Isermann et al., 2004; Bhatla and Horvitz, 2015). We conclude that the responses of PRDX-2 to oxidative stress are cellular context-dependent.

SKN-1 controls expression of PRDX-2 in the gut, but not in neurons

This prompted us to test whether PRDX-2 expression could rely on different subcellular regulations. By analogy with yeast, we wondered whether PRDX-2 would be controlled by the Yap1 nematode orthologue SKN-1 (Blackwell et al., 2015) in cells where PRDX-2 is induced upon oxidative stress, and asked whether such regulation occurs in other cells. We sought to test this hypothesis by inactivating the function of SKN-1 in the PRDX-2::GFP knock-in line. We first used the *skn-1(zj15)* allele, which inactivates specifically the gut-specific isoforms, leaving neuronal isoforms unaffected (Tang et al., 2016). In this mutant, the basal expression level of PRDX-2 is reduced in the foregut, but a weak induction persists after a 10mM H_2O_2 treatment (Fig. 2C), suggesting that the neuronal isoforms could mediate this effect. Consistent with this, the RNAi-mediated knock-down of all *skn-1* isoforms also triggered a reduction of PRDX-2::GFP signal in the anterior gut and an absence of induction upon H_2O_2 treatment (Fig. 2B,D). This result indicates that SKN-1 activity is essential to regulate PRDX-2 expression in the anterior gut, both at the basal level and under oxidative stress. In agreement with this, SKN-1 was found to bind to the *prdx-2* promoter in chromatin immunoprecipitation experiments coupled with high-throughput DNA sequencing (ChIP-seq) (Niu et al., 2011) (Fig. 2E).

In contrast, in I2 neurons, no change in the PRDX-2 level was detected at the basal level or after H_2O_2 treatment compared to controls, neither in *skn-1(zj15)* mutants nor in *skn-1(RNAi)* animals (sup. Fig. 2). With the limitation that RNAi efficiency may be lower in neurons (Calixto et al. 2010), we suggest that additional transcription factor(s) might regulate *prdx-2* expression in these neurons. Consistently, multiple transcription factors were reported to bind to the *prdx-2* promoter by ChIP-seq (Niu et al., 2011) (Fig. 2E).

We conclude that *skn-1* accomplishes a cell autonomous regulation of *prdx-2* in the intestine, but this regulation may not occur in neurons, where PRDX-2 is expressed. Taken together, our data suggest that PRDX-2 might exert a different function depending on the cell type: H_2O_2 detoxification in the foregut, triggered by SKN-1, *vs.* H_2O_2 perception or signaling in I2 neurons.

PHA neurons respond to H_2O_2 in a prdx-2-dependent manner

As PRDX-2 is expressed in other neurons than I2s, we asked whether PRDX-2 endows these neurons with oxidative stress sensing properties. We focused on PHA tail neurons, as they belong to the phasmid sensory sensilla and respond to many noxious stimuli (Zou et al., 2017). We monitored PHA neuron activation by imaging calcium using the GCaMP3 fluorescent sensor (Tian et al., 2009) expressed under the *flp-15* promoter, specific to I2 and PHA neurons (Kim and Li, 2004).

To image calcium fluxes in neurons, L4 animals were trapped in microfluidic chambers and exposed to H_2O_2 (Fig. 3A, sup. Fig. 3), and their response was followed in 4D spinning-disc ultrafast acquisitions. This experimental setup, combined with semi-automated image analyses to quantify the mean fluorescence in neurons over time, confirmed the activation of I2s upon a 1mM H_2O_2 treatment (Fig. 3B-D, movie 1), similar to that observed upon exposure to H_2O_2 vapor (*ie.* 8.82M, Bhatla and Horvitz, 2015). As PRDX-2 reproducibly shows an asymmetric expression level in I2L and I2R (Fig. 1B,D), each neuron was scored individually to take into account a putative left-right effect. However, this did not impact neuron response as no significant difference in the normalized response of left and right neurons was noticed (Fig. 3B,C,L). Importantly, we observed that PHA neurons respond to 1mM H_2O_2 comparably to I2 neurons (Fig. 3C,D,H, movie 2). We then investigated whether PRDX-2 function was necessary for PHA response, using a strong *prdx-2* loss of function mutant. In agreement with previous work (Bhatla and Horvitz, 2015), I2 neurons in *prdx-2(gk169)* mutants failed to respond to 1mM H_2O_2 (Fig 3E-H, movie 3). Interestingly, we uncovered that PHA neuron response was severely impaired in *prdx-2* mutants, although not completely abolished as in I2s (Fig. 3E,G,H, movie 4). From these observations, we conclude that both I2s and PHAs responses to oxidative stress require the function of the peroxiredoxin PRDX-2, but the residual response of PHA neurons suggests a lesser requirement of the antioxidant in tail neurons.

I2s and PHAs show differences in H_2O_2 sensitivity and in receptors involved

Given the putative role of PRDX-2 as an H_2O_2 sensor, the fact that there was a slight difference in PRDX-2 activity requirement in I2s and PHAs prompted us to analyze whether the head and tail neurons share the same sensitivity to H_2O_2. We thus tested whether I2 and PHA neurons exhibit a response to the very mild dose of 10µM H_2O_2. Indeed, at this dose, it

has been reported that only a minority of animals (≈ 35%) respond by inhibiting pharyngeal pumping (Bhatla and Horvitz, 2015). In our experiments, whereas I2 neurons failed to be activated in most animals at 10µM H_2O_2 (25/29, Fig. 3I,J,L, movie 5), PHA neurons responded in the vast majority of animals (25/27, Fig. 3I, movie 6), in a similar manner than at 1mM H_2O_2 (Fig. 3K,L). We conclude that PHA neurons are more sensitive to low doses of H_2O_2 than I2 neurons.

The difference in sensitivity between I2 and PHA neurons may come from distinct molecular mechanisms. To explore this possibility, we first tested which receptors are required in I2s and in PHAs for H_2O_2 perception. We focused on photoreceptors as photosensation is likely to involve the generation of ROS (Bhatla and Horvitz, 2015; Zhang et al., 2020). In *C. elegans*, light sensing relies on unusual gustatory G-protein-coupled receptors (GPCRs) related to vertebrate photoreceptors: the two nematode closest paralogs LITE-1 and GUR-3 mediate photosensation in ASJ and ASH neurons (Liu et al., 2010; Ward et al., 2008; Zhang et al., 2020), and light and H_2O_2 sensing in I2 neurons (Bhatla and Horvitz, 2015). We investigated whether these two receptors are differentially localized in I2 and PHA neurons. We generated a knock-in GUR-3::GFP line, which revealed that GUR-3 is solely expressed in I2 and I4 photosensory neurons (Fig. 4A), as previously reported using episomal expression (Bhatla and Horvitz, 2015). Such a restricted pattern deeply contrasts with the broad expression domain of LITE-1, which includes phasmid neurons (PHA and PHB), but not I2 neurons, as shown using both translational and transcriptional reporters (Bhatla and Horvitz, 2015).

These differential localizations prompted us to inquire whether mutants in these receptors were still able to trigger a response to 1mM H_2O_2 in I2 and PHA neurons. In *gur-3(ok2245)* mutants, only PHA neurons were able to respond to 1mM H_2O_2 (Fig. 4B,C, sup. Fig. 4, movies 7,8), providing evidence that GUR-3 function is not essential in PHA neurons for H_2O_2 sensing. In contrast, *lite-1(ce314)* mutants showed a reciprocal response, with only I2 neurons activated upon 1mM H_2O_2 exposure (Fig. 4B,C, sup. Fig. 4, movies 9,10). In conclusion, H_2O_2 likely activates I2 neurons via *gur-3* and PHA neurons via its paralog *lite-1,* respectively. Interestingly, these observations might explain the previously reported impaired avoidance response of *lite-1* mutants to 1mM H_2O_2 (Bhatla and Horvitz, 2015), as PHA neurons are involved in escape behavior (Hilliard et al., 2002)**.**

PMK-1 is required for PHAs response to H_2O_2 but seems dispensable in I2s

Since H_2O_2 perception in I2 and PHA neurons involves different receptors and requires the function of PRDX-2 in both cases, we wondered what type of signaling occurs downstream PRDX-2 to trigger neuronal activation upon H_2O_2 stimulation.

As mentioned above, studies in various models have reported that peroxiredoxins can modulate the p38/MAPK signaling pathway to influence cellular decisions, notably in drosophila and mammalian cells (Barata and Dick, 2020). In *C. elegans*, specifically, the activation of this PRDX-2-PMK-1/p38 cascade allows micromolar doses of H_2O_2 to potentiate the ASH neuron sensory behavior to glycerol (Li et al., 2016). Therefore, we tested a potential requirement of the PMK-1/p38 MAPK function in H_2O_2 sensing in I2s and PHAs by analyzing their responses in a *pmk-1* loss-of-function genetic background. As the strongest allele *pmk-*

1(ok811) is a homozygous lethal deletion, we had to use the hypomorphic *pmk-1(km25)* viable mutant, which carries an N-terminal deletion, generating a truncated version of PMK-1 (Mizuno et al., 2004). In *pmk-1(km25)* mutants, while I2 neurons responded to 1mM H_2O_2, PHA neurons showed an attenuated response to 1mM H_2O_2 compared to controls (Fig. 4D,E, movies 11, 12). Therefore, PMK-1 seems dispensable in I2 neurons for 1mM H_2O_2 sensing but plays a role in PHA neurons response.

In ASH neurons, the activation of p38/PMK-1 leads to the phosphorylation of the voltage-gated calcium channel OSM-9; resulting in improved neuronal sensitivity (Li et al., 2016). Given the differential requirement of PMK-1 in I2 and PHA neurons, we then asked whether p38/PMK-1 could promote PHA sensitivity to low doses of H_2O_2, as in ASH neurons. We thus examined PHA neuron response to 10µM H_2O_2 in *pmk-1(km25)* mutants, and found that it was abolished (Fig 4D,F, movies 13,14). We conclude that PMK-1/p38MAPK activity is required for PHA neurons hypersensitivity to H_2O_2, whereas it seems dispensable in I2 neurons.

PHA neurons are photosensory neurons like ASH neurons

Light sensing has been reported for ASJ, ASH and I2 neurons and require either the LITE-1 or the GUR-3 receptor, respectively (Bhatla and Horvitz, 2015; Liu et al., 2010; Ward et al., 2008; Zhang et al., 2020). As PHAs neurons require LITE-1 to respond to H_2O_2 (Fig. 4B,C), we asked whether they could respond to light. To test this, we monitored calcium transients in three neuronal compartments using the GCaMP strain upon stimulating neurons with blue light, as previously done for I2 or ASH neurons (Bhatla and Horvitz, 2015; Zhang et al., 2020). Interestingly, we found that all regions of PHA neurons responded to light, displaying a different response profile than those of I2 neurons (Fig. 4G,H, movies 15,16,17): PHA soma showed a stronger and longer response than I2 soma; PHA posterior neurite responded much slower that in I2 where it exhibits the fastest and strongest response peak, and the anterior neurite also had a slower recovery than in I2. Overall, while I2 neurons exhibit a fast photoresponse within 10-15s, PHA neurons photoresponse requires twice longer to return to steady state (approx. 30s). Strikingly, we noticed that PHA neurons profile is highly reminiscent of that reported in ASH neurons photoresponse (Zhang et al., 2020).

Discussion

H_2O_2 sensing in head and tail neurons relies on different mechanisms

Here, we describe how two pairs of sensory neurons located in the head and the tail of *C. elegans*, namely I2s and PHAs, contribute to exogenous H_2O_2 sensing. Compared to previous reports, our study relies on a PRDX-2::GFP knock-in line more closely reflecting endogenous expression level, in comparison to overexpression often observed with extrachromosomal arrays. While classical methods do not enable precise control of the environment such as application of a stress, we carried out neuron response experiments using the microfluidic technology, allowing live imaging of immobilized animals upon simultaneous exposure to a controlled oxidative stress.

We found that PHA tail neurons can elicit a response to a micromolar range of H_2O_2, whereas I2 head neurons cannot, suggesting that distinct molecular mechanisms may account for this difference. Accordingly, while the peroxiredoxin PRDX-2 is essential for H_2O_2 sensing in both I2 and PHA neurons, each neuron pair seems to require a different transmembrane receptor to transduce the signal: I2 neurons rely on activity of the gustatory receptor GUR-3, while PHA neurons would require its paralogue LITE-1. Finally, we found that p38/PMK-1 activity would be specifically required in PHA neurons to confer their hypersensitivity to H_2O_2, but dispensable in I2 neurons.

Overall, our data are consistent with previous findings unveiling the existence of two distinct modes of response to oxidative stress in *C. elegans*: a direct response in peripheral tissues such as the gut, and a neuronally-regulated response relying on synaptic transmission (Rangaraju et al., 2015). Specifically, we uncovered that a harsh oxidative stress (10mM H_2O_2) triggers stress response in the anterior gut and in the EPC (Figs. 1-2) through PRDX-2 induction, while a lower dose of H_2O_2 (1mM) triggers I2 and PHA neuron activation (Fig. 3). Interestingly, both types of response involve the peroxiredoxin PRDX-2, which behaves differently in the two cellular contexts: PRDX-2 was found to be cell-autonomously induced by SKN-1 in the intestine, but likely not in neurons. Therefore, we propose that in the gut PRDX-2 might act as a peroxidase, as proposed (Oláhová et al., 2008), whereas it could function as a H_2O_2-signaling molecule in neurons, as suggested for I2 neurons (Isermann et al., 2004, Bhatla and Horvitz, 2015). Importantly, H_2O_2 response in I2 and PHA neurons requires the joint function of PRDX-2 and a receptor, as each mutant individually cannot respond (Figs. 3-4). In addition, former rescue experiments indicated that light response in I2 requires the activity of PRDX-2 and GUR-3 in I2 neurons (Bhatla and Horvitz, 2015). Based on all these data and recent studies shedding light on how H_2O_2 is sensed in plant and animal cells (Barata and Dick, 2020; Wu et al., 2020), we propose new hypotheses regarding H_2O_2 signaling in neurons which are depicted in Fig. 5 and described below, to integrate our findings with recent results from the literature.

A presumptive model of H_2O_2 sensing in C. elegans neurons

In both I2 and PHA neurons, we favor the hypothesis that cytosolic PRDX-2 rather than the transmembrane receptor would be the neuronal H_2O_2 sensor, based on the following observations: i) in many cases, H_2O_2 signaling is mediated by oxidation of cysteines in redox-regulated proteins (Groitl and Jakob, 2014). Alternatively, redox signaling often relies on a cascade involving peroxiredoxins as a sensor and transducer of H_2O_2 signal (Stöcker et al., 2018). It has been proposed that thiol modifications would be much faster when catalyzed by peroxiredoxins (Flohé, 2016; Netto and Antunes, 2016; Randall et al., 2013), due to their relative abundance and their very high reactivity towards H_2O_2 (Winterbourn and Peskin, 2016). Here, the striking abundance of PRDX-2 in PHA and especially in I2 neurons seen in the GFP-tagged *prdx-2* knock-in line reinforces this idea, as well as the quasi-absence of H_2O_2 response in *prdx-2* mutants. Interestingly, LITE-1-dependent photosensation in ASH neurons requires thioredoxin (Zhang et al., 2020), suggesting redox signal transduction through antioxidants of the peroxiredoxic cycle; and LITE-1-dependent ASJ photosensory neurons also express the TRX-1 thioredoxin (Miranda-Vizuete et al., 2006). Therefore, we propose that H_2O_2 signaling in I2 and PHA would involve a redox signaling cascade through PRDX-2. ii) Concerning receptor topology, GUR-3 and LITE-1 present a relatively small extracellular domain —poorly conserved compared to its intracellular part— devoid of any conserved cysteine.

Remarquably, conserved cysteines between LITE-1 and GUR-3 are only found in the first and third intracellular loops and in the fifth transmembrane domain (Fig. 5A,B). This structure is reminiscent of the vertebrate transmembrane protein GDE2, which is activated intracellularly by the Prdx1 peroxiredoxin to induce motor neuron differentiation (Yan et al., 2009); but it sharply contrasts with that of the recently identified H_2O_2 sensor in plants, the HCPA1 receptor (Wu et al., 2020). HCPA1 possesses a large extracellular domain with many cysteines, which when directly oxidized by H_2O_2, induces a conformation change, in the receptor, hence HCPA1 activation and subsequent calcium intracellular entry. Here, GUR-3 and LITE-1 receptor topology does not support the hypothesis of a direct oxidation by H_2O_2 on the extracellular domain, but rather suggests intracellular signaling as in the case of GDE2.

Taken together, we thus propose a scenario in which H_2O_2 would diffuse through the neuron plasma membrane and oxidize PRDX-2. Oxidized PRDX-2 or its disulfide form (PRDX-$2^{ox/S\text{-}S}$) would in turn activate GUR-3 in I2s, or LITE-1 in PHAs, through the cysteines of their intracellular domain, *eg*. by inducing a conformation change upon the formation of a disulfide bond or by forming a transient disulfide bond conjugate (Fig. 5A,B). Once GUR-3 or LITE-1 becomes activated by PRDX-2^{ox}, this likely triggers action potentials upon the opening of voltage-gated calcium channels and neurotransmitter release, likely inducing the appropriate behavior (Fig. 5C,D). Interestingly, the voltage-gated calcium channels have been reported to be different in the two neuron pairs: whereas I2 activation depends in part on the voltage-gated calcium channels UNC-2 and UNC-36 (Bhatla et al., 2015); PHA neurons calcium transients rely on both the cyclic nucleotide-gated channel TAX-4 and on OSM-9, the nematode equivalent of vertebrate TRPV5 (i.e., transient receptor potential vanilloid cation channel subfamily V member 5) (Zou et al., 2017). In addition, the other TRPV5 channel subunit OCR-2 may also act in PHAs, as it functions in a cooperative association with OSM-9 (Ohnishi et al., 2020), and OCR-2 is expressed in PHAs (Jose et al., 2007)(sup. Fig. 8). Therefore, although they are closely related and can both sense H_2O_2 and light, GUR-3 and LITE-1 signaling seems to rely on different downstream transducers. Thus, except for the requirement of PRDX-2, which might trigger H_2O_2-mediated receptor activation, I2 and PHA neurons would use distinct molecular pathways to transduce H_2O_2 response.

A striking parallel between PHA and ASH neurons

Our data uncover a high sensitivity of PHAs to micromolar doses of H_2O_2 that is not seen in I2 neurons, which requires PMK-1/p38 activity. Strikingly, micromolar doses of H_2O_2 increase the sensitivity of ASH neurons to glycerol through the PRDX-2-mediated activation of the PMK-1/p38 pathway (Li et al., 2016), which results in the terminal phosphorylation of the TRPV sensory channel OSM-9, likely increasing its sensitivity (Li et al., 2016). Although our study and the latter do not elucidate how PRDX-2 triggers PMK-1 activation, recent evidence sheds light on this process: in both mammalian and drosophila cells, H_2O_2 induces transient disulfide-linked conjugates between the MAP3K and a typical 2-Cys peroxiredoxin (Barata and Dick, 2020). Similarly, in *C. elegans*, PRDX-2 could activate the MAPKKK NSY-1, as NSY-1 function is required in ASH neuron for H_2O_2-behavioral induced potentiation (Li et al., 2016), and it may be expressed in PHAs (*unidentified cells of the tail, D. Moerman, WormBase*). Based on these observations and on the fact that OSM-9 is expressed (Colbert et al., 1997) and likely required in PHA neurons (Zou et al., 2017), we propose that PMK-1 function might increase PHA neurons' sensitivity to H_2O_2, potentially through the downstream phosphorylation of

OSM-9, as in ASH neurons (Fig. 5D). These assumptions, which will necessitate further experimental validations, are supported by the observation that ASHL/R and PHAL/R are both descendants of ABplp or ABprp in the nematode cell lineage, and hence may express similar sets of genes following lineage-specific priming (Charest et al., 2020). In addition, the fact that PHA, PHB and ASH were found in the same neuron cluster by (Lorenzo et al., 2020), further suggests that they share similar molecular signatures. To illustrate the parallel between ASH and PHA polymodal nociceptors, we retrieved the set of genes expressed in these neurons from (Lorenzo et al 2020)'s dataset, and analysed which genes were specifically enriched in these two neurons in comparison to all other neurons (sup. Fig. 8). This analysis revealed that ASH and PHA not only express many genes specific to ciliated neurons, as expected (*eg*. *che-3, nphp-4, che-11*, *ifta-1*; C33A12.4 and R102.2, (Kunimoto et al. 2005)) but also a number of common receptors (*eg. ocr-2, osm-9, ida-1, casy-1, ptp-3* or *pdfr-1*) although some of them are more enriched in ASH (*dop-2, nrx-1, snt-5, sue-1*). Intriguingly, their neuropeptide profile appears slightly different for the two neuron pairs (PHA enriched in *flp-7, flp-4, flp-16, nlp-1 ins-18,* while ASH strongly express *flp-13* and *npr* genes), suggesting that beyond their functional similarity, ASH and PHA may trigger different types of intercellular communication. Finally, this analysis highlights that several genes with unknown function are highly enriched in both ASH and PHA (*eg*. F27C1.11, W05F2.7, *tos-1, cab-1*, sup. Fig. 8), pointing to their potential importance in neuronal function.

Taken together, our analyses highlight the common features shared between PHA and ASH polymodal nociceptive neurons, as formerly noticed (Hilliard et al., 2002), since they both: i) display a higher sensitivity dependent on the PMK-1/p38 pathway (Fig. 4F and (Li et al., 2016), ii) exhibit a similar profile of response to light (Fig. 4H and (Zhang et al., 2020), iii) require the photoreceptor LITE-1 for lightsensing (Zhang et al., 2020) or H_2O_2 sensing (Fig 4BC), iv) trigger avoidance (Hilliard et al., 2002), and v) were found in the same class of gene-expressing neurons and therefore share a close molecular signature (Lorenzo et al., 2020), sup. Fig. 8). These observations led us to propose that the nematode might integrate the environmental redox signals from at least three different pairs of neurons (I2, ASH, PHA) in order to trigger an appropriate dose-dependent physiological response. To our knowledge, the sensitivity of PHA neurons to light and to a low H_2O_2 concentration has never been described.

GUR-3 and LITE-1 receptors mediate both light and H_2O_2 sensing

In yeast, light sensing relies on the peroxisomal oxidase Pox1 which triggers light-dependent H_2O_2 formation, the latter being sensed by the Tsa1 peroxiredoxin and transduced to thioredoxin for subsequent signaling (Bodvard et al., 2017). Nematodes, unlike yeast, require a photoreceptor in addition to the antioxidant for lightsensation: GUR-3 in I2 neurons (Bhatla and Horvitz, 2015), and LITE-1 in ASJ and ASH neurons (Liu et al., 2010; Zhang et al., 2020). Here we showed that both I2 and PHA respond to light, but with a different profile. Despite its unusual membrane topology, LITE-1 has been shown to encode a bona fide photoreceptor, whose photoabsorption depends on its conformation (Gong et al., 2017). However, whether light directly activate the neuron photoreceptor or triggers intracellular H_2O_2 release and signaling is still unclear. In agreement with the fact that H_2O_2 inhibits LITE-1 photoabsorption *in vitro* (Gong et al., 2017), it has been shown that a H_2O_2 pretreatment reduces LITE-1-mediated photoresponse in ASH neurons (Zhang et al., 2020). Consistent with

these reports, our data illustrate for the first time that GUR-3 and LITE-1 have a dual function in both light and H_2O_2 sensing and open up the hypothesis that, as in yeast, redox signaling could be involved in transducing the light signal, as for H_2O_2 sensing (Fig. 5). We observed that PHA and ASH neurons exhibit a similar type of reponse to light (Fig 4H and (Zhang et al., 2020), which is slower than that observed in I2 neurons (Fig. 4G and Bhatla and Horvitz 2015). Whether this difference depends on the photoreceptor (LITE-1 in PHA and ASH *vs* GUR-3 in I2), or on its downstream redox signaling cascade, would be worth investigating.

Finally, it is noteworthy that some neurons rely on peroxiredoxin for oxidative stress and/or light sensing, such as I2 or PHA, while others rely on thioredoxin, such as ASJ, or ASH for light sensing. This further underlines the importance of redox signaling relays involving antioxidants of the peroxiredoxic cycle in these photosensory neurons of the nematode.

In conclusion, our work illustrates that nematodes can sense various concentrations of H_2O_2 through sensory neurons located in the head and the tail, using either partially different (I2 and PHA), or similar molecular mechanisms (ASH and PHA). This set of neurons also confer light sensing to the nematode with a distinct speed in the response (fast in I2, slow in PHA and ASH, (Zhang et al., 2020)). While I2 neurons seem more specialized in sensing oxidative stress (Bhatla and Horvitz, 2015; Yemini et al., 2021), PHA and ASH can detect many other stimuli (Zou et al, 2016), but all of them can trigger avoidance. These observations may help uncover whether and how inputs from head and tail oxidative stress sensory neurons integrate to allow nematodes to quickly and appropriately react to a sudden change in the environment.

Experimental procedures

Generation of plasmids and transgenic strains by CRISPR/Cas9-mediated genome editing

C. elegans strains (listed in Table S1) were maintained as described (Brenner, 1974). PRDX-2::GFP knock-in strain was generated by CRISPR/Cas9-mediated genome editing, using a DNA plasmid-based repair template strategy (Dickinson et al., 2013). For both PRDX-2 and GUR-3 knock-ins, a C-terminal GFP fusion was generated, comprising a flexible linker between the coding region and GFP to allow correct folding of the fusion protein. A combined small guide-RNA/repair template plasmid was built using the SAP Trap strategy (Schwartz and Jorgensen, 2016). Phusion DNA polymerase was used to amplify by PCR 5' and 3' *prdx-2* and *gur-3* homology arms (HAs) from N2 genomic DNA, using primers containing SapI restriction sites and silent mutations to prevent Cas9 re-cleavage (primers listed in Supplemental Table 2). After purification, 5' and 3' HAs and sgRNA oligonucleotides were assembled into the destination vector (pMLS256), together with the flexible linker (from pMLS287), GFP and the *unc-119* rescuing element (from pMLS252), in a single SapI restriction-ligation reaction, as described (Schwartz and Jorgensen, 2016). Prior to transformation in DH5α cells, a sabotage restriction was performed with SpeI to digest empty destination vectors but not the desired assembly constructs, which were subsequentially verified by restriction digest analysis and sequencing. All plasmids used for injection were purified using a DNA Miniprep Kit (PureLink, Invitrogen), or a DNA midiprep kit (Macherey Nagel). For PRDX-2::GFP knock-in, a plasmid mix containing combined sgRNA/repair template plasmid (50 ng/µl), Cas9-encoding pSJ858 (25ng/µl) and co-injection markers (pCFJ90 at 2.5ng/µl; pCFJ104 at 5ng/µl, and pGH8 at 5ng/µl) was injected in the germline of *unc-119(ed3)* animals (Dickinson et al., 2013). For GUR-3::GFP knock-in, an injection mix containing purified Cas9 protein (IDT) associated with tracrRNA and crRNA (guide RNA), GUR-3 repair template, and co-injection markers was injected in *unc-119(ed3)* animals, according to IDT online protocols for *C. elegans*. Plates containing 2/3 injected F0 animals were starved, chunked on fresh plates, for candidates screening (attested by the presence of wild-type non fluorescent animals). Knock-in events were validated by PCR on homozygous lysed worms (QuantaBio AccuStart II GelTrack PCR SuperMix), using primers annealing in the inserted sequence and in an adjacent genomic region not included in the repair template. The PRDX-2::GFP strain was outcrossed 5 times to N2 wild-types.

RNA interference

RNAi experiments were performed by feeding using the Ahringer-MRC feeding library (Kamath et al., 2003). Animals fed with the empty vector L4440 served as a negative control. The efficiency of each RNAi experiment was assessed by adding an internal positive control, *zyg-9(RNAi)*, which induces embryonic lethality.

Spinning-disk confocal microscopy acquisitions and fluorescence intensity measurements

For live imaging, animals were anesthetized in M9 containing 1mM levamisole and mounted between slide and coverslip on 3% agarose pads. Synchronized L4 animals were

treated for 30min in a 96-well flat bottom plate, in 50µl of M9 containing 1mM or 10mM H_2O_2. Treated animals were transferred using a siliconized tip on a freshly seeded plate to recover, and imaged 1h30 to 2h later. Spinning-disk confocal imaging was performed on a system composed of an inverted DMI8 Leica microscope, a Yokogawa CSUW1 head, an Orca Flash 4.0 camera (2048*2018 pixels) piloted by the Metamorph software. Objective used were oil-immersion 40X (HC PL APO, NA 1.3) or 63X (HCX PL APO Lambda blue, NA 1.4). The temperature of the microscopy room was maintained at 20 ˚C for all experiments. Z-stacks of various body regions were acquired with a constant exposure time and a constant laser power in all experiments. Maximum intensity projections were used to generate the images shown. Fluorescence intensity measurements in int1, I2 and EPC cells were performed using the Fiji software, by manually drawing a region of interest (ROI) around the cell (int1, EPC), or applying a threshold (I2 neurons), background was subtracted and average pixel intensity was quantified.

Microfabrication and microfluidic chip preparation

The microfluidic chip original design was inspired by the the Wormspa (Kopito and Levine, 2014), but pillars distances were adapted to trap L4 animals, and multiple series of traps were included to increase the number of experiments per chip (sup. Fig. 3). A master mold was made by standard soft photolithography processes by spin-coating a 25µm layer of SU-8 2025 (Microchem, USA) photoresist at 2700 rpm for 30sec on a 3" wafer (Neyco, FRANCE). Then, we used a soft bake f 7min at 95°C on hot plates (VWR) followed by a UV 365nm exposure at 160 mJ/cm² with a mask aligner (UV-KUB3 Kloé®, FRANCE). Finally, a post-exposure baking identical to the soft bake was performed before development with SU-8 developer (Microchem, USA). Then, the wafer was baked at 150°C for 15min to anneal potential cracks and strengthen the adhesion of the resist to the wafer. Finally, the master mold was treated with chlorotrimethylsilane to passivate the surface.

Worm microchannels were cast by curing PDMS (Sylgard 184,10:1 mixing ratio), covalently bound to a 24 × 50 mm coverslip after plasma surface activation (Diener, Germany), and incubated 20min at 60°C for optimal adhesion. The chip was perfused with filtrated M9 solution through the medium inlet using a peristaltic pump (Ismatec), until complete removal of air bubbles. Worm loading was performed with the pump set at a low flow rate (<30 µl/min), through a distinct inlet (sup. Fig. 3): 10-15 young L4 animals (synchronized by bleaching 48h prior to each experiment) were picked in a siliconized Eppendorf tube containing M9, and perfused into the traps. The loaded chip was carried to the microscope while being still connected to the pump by a gravity flow (preventing animals to escape) until the microfluidic chip was installed on the microscope stage.

Calcium imaging

I2 and PHA neuronal response was monitored using the calcium sensor GCaMP3 expressed under the *flp-15* promoter as in (Bhatla and Horvitz, 2015). To image H_2O_2 response, young L4 animals trapped in microfluidic chips were imaged using the confocal spinning disc system described above with the 20X air objective (HC PL APO CS2, NA 0.75). The microfluidic chip allowed the simultaneous recording of up to 3 animals per experiment (sup. Fig. 3). Z-stacks of 10-15 images (10 µm spacing) were acquired every 2s (using the stream Z mode), for

350 time points. Exposure time was 50ms and laser power set on 40%. The device was perfused with M9 medium throughout the experiment using a peristaltic pump set at 80 µl/min, and H_2O_2 was perfused (at 10µM or 1mM in M9) for 100 time points (3min20s) after an initial recording of 35-45 time points. Movies were computationally projected using MetaMorph, and data processing (including movie registration, neuron segmentation and tracking over time) was conducted with a custom-developed Matlab program detailed below and available at https://github.com/gcharvin/viewworm (a user guide is provided in supplemental Methods).

To image light response in I2 and PHA neurons, L4 worms were mounted on a slide covered with 3% agarose pads in M9 supplemented with 1mM levamisole. Video-recordings were performed on the spinning-disc microscope using the 40X oil objective. Animals were exposed to blue light (485nm) while their neuronal response was simultaneously recorded in stream mode (10 frames/sec, single Z, 100ms exposure, laser 100%) for 30sec.

Calcium response analyses

For H_2O_2 response analyses, sequences of images were spatially realigned with respect to the first image of the timeseries in order to limit the apparent motion of the worm in the trap and ease the tracking of neurons of interest. This image registration process was performed using standard 2D image cross-correlation by taking the first image as a reference. Then, we used a machine-learning algorithm (based on a decision tree) to segment pixels in the fluorescent images. For this, we took a series of image transforms (gaussian, median, range filters) as descriptors for the classifier, and we trained the model on typically 10 frames before applying the result to the rest of the time series. This segmentation method appeared to be superior to simple image thresholding, which is inadequate when dealing with fluorescent signals that vary both in time and space (the brightness of two neurons is quite different). Next to the segmentation procedure, we tracked the identified neurons using distance minimization, and we quantified the mean fluorescence signal in each neuron over time. Last, fluorescence data corresponding to individual animals were pooled after synchronization from the time of exposure to H_2O_2 and signal normalization. This image analysis pipeline is available at https://github.com/gcharvin/viewworm and a tutorial for use is included in supplemental methods. As some movies could not be quantified due to uncontrolled animal movements, a visual classification of neuronal responses (high, moderate, absent) was made by comparison to successfully tracked movies.

For light response analyses in I2 and PHA neurons, the same image processing pipeline as in (Bhatla and Horvitz, 2015) was used, except that ROI were manually drawn in Fiji.

Statistical analyses

P-values were calculated with an unpaired two-tailed Student test; the Welsh correction was applied when the two samples had unequal variances. Error bars depict standard deviation in all figures. Statistical analyses were conducted with the GraphPad Prism9 software. The data presented here come from at least three independent experiments. For p values, not significant $p>0.05$; *$p<0.05$; **$p<0.01$; ***$p<0.001$: ****$p<0.0001$.

Acknowledgements

We are grateful to all the staff members of the Imaging Center of the IGBMC, especially Elvire Guiot, Erwan Grandgirard and Bertrand Vernay for assistance in confocal microscopy. We thank Christelle Gally, Basile Jacquel and Eric Marois for helpful discussions and critical reading of the manuscript, and Sandra Bour for assistance with figure design. We are indebted to the Reymann, Vermot and Jarriault labs for sharing their equipments and reagents. We thank the Horvitz lab, especially Na An, for providing the MT GCaMP strains. We thank WormBase and the *Caenorhabditis* Genetics Center (funded by NIH Office of Research Infrastructure Programs P40 OD010440, University of Minnesota) for providing strains.

Funding

This work was funded by the grant ANR-10-LABX-0030-INRT, a French State fund managed by the Agence Nationale de la Recherche under the frame program Investissements d'Avenir ANR-10-IDEX- 0002-02.

Author contributions

S.Q. designed and conducted the experiments, analyzed data and wrote the manuscript; T.A. designed and printed the microfluidic chip; T. Y. contributed to ChIP seq data analyses; G.C. developed the Matlab pipeline for data analyses.

Conflict of interest

The authors declare no competing interest.

References

Back, P., De Vos, W.H., Depuydt, G.G., Matthijssens, F., Vanfleteren, J.R., and Braeckman, B.P. (2012). Exploring real-time in vivo redox biology of developing and aging Caenorhabditis elegans. Free Radic. Biol. Med. *52*, 850–859.

Barata, A.G., and Dick, T.P. (2020). A role for peroxiredoxins in H2O2- and MEKK-dependent activation of the p38 signaling pathway. Redox Biol *28*, 101340.

Bhatla, N., and Horvitz, H.R. (2015). Light and hydrogen peroxide inhibit C. elegans Feeding through gustatory receptor orthologs and pharyngeal neurons. Neuron *85*, 804–818.

Bhatla, N., Droste, R., Sando, S.R., Huang, A., and Horvitz, H.R. (2015). Distinct Neural Circuits Control Rhythm Inhibition and Spitting by the Myogenic Pharynx of C. elegans. Curr. Biol. *25*, 2075–2089.

Blackwell, T.K., Steinbaugh, M.J., Hourihan, J.M., Ewald, C.Y., and Isik, M. (2015). SKN-1/Nrf, stress responses, and aging in Caenorhabditis elegans. Free Radic. Biol. Med. *88*, 290–301.

Bodvard, K., Peeters, K., Roger, F., Romanov, N., Igbaria, A., Welkenhuysen, N., Palais, G., Reiter, W., Toledano, M.B., Käll, M., et al. (2017). Light-sensing via hydrogen peroxide and a peroxiredoxin. Nat. Commun. *8*, 14791.

Breker, M., Gymrek, M., and Schuldiner, M. (2013). A novel single-cell screening platform reveals proteome plasticity during yeast stress responses. J. Cell Biol. *200*, 839–850.

Brenner, S. (1974). The genetics of Caenorhabditis elegans. Genetics *77*, 71–94.

Cao, J., Packer, J.S., Ramani, V., Cusanovich, D.A., Huynh, C., Daza, R., Qiu, X., Lee, C., Furlan, S.N., Steemers, F.J., et al. (2017). Comprehensive single-cell transcriptional profiling of a multicellular organism. Science *357*, 661–667.

Chae, H.Z., Kim, H.J., Kang, S.W., and Rhee, S.G. (1999). Characterization of three isoforms of mammalian peroxiredoxin that reduce peroxides in the presence of thioredoxin. Diabetes Res. Clin. Pract. *45*, 101–112.

Charest, J., Daniele, T., Wang, J., Bykov, A., Mandlbauer, A., Asparuhova, M., Röhsner, J., Gutiérrez-Pérez, P., and Cochella, L. (2020). Combinatorial Action of Temporally Segregated Transcription Factors. Dev. Cell *55*, 483-499.e7.

Cobb, C.A., and Cole, M.P. (2015). Oxidative and nitrative stress in neurodegeneration. Neurobiol. Dis. *84*, 4–21.

Colbert, H.A., Smith, T.L., and Bargmann, C.I. (1997). OSM-9, a novel protein with structural similarity to channels, is required for olfaction, mechanosensation, and olfactory adaptation inCaenorhabditis elegans. Journal of Neuroscience.

Davalli, P., Mitic, T., Caporali, A., Lauriola, A., and D'Arca, D. (2016). ROS, Cell Senescence, and Novel Molecular Mechanisms in Aging and Age-Related Diseases. Oxid. Med. Cell. Longev. *2016*, 3565127.

Dickinson, D.J., Ward, J.D., Reiner, D.J., and Goldstein, B. (2013). Engineering the Caenorhabditis elegans genome using Cas9-triggered homologous recombination. Nat. Methods.

Ding, C., Fan, X., and Wu, G. (2017). Peroxiredoxin 1 - an antioxidant enzyme in cancer. Journal of Cellular and Molecular Medicine *21*, 193–202.

Flohé, L. (2016). The impact of thiol peroxidases on redox regulation. Free Radic. Res. *50*, 126–142.

Gomes, L.C., Odedra, D., Dikic, I., and Pohl, C. (2016). Autophagy and modular restructuring of metabolism control germline tumor differentiation and proliferation in C. elegans. Autophagy *12*, 529–546.

Gong, J., Yuan, Y., Ward, A., Kang, L., Zhang, B., Wu, Z., Peng, J., Feng, Z., Liu, J., and Xu, X.Z.S. (2017). The C. elegans Taste Receptor Homolog LITE-1 Is a Photoreceptor. Cell *168*, 325.

Goodman, M.B., and Sengupta, P. (2019). How Caenorhabditis elegans Senses Mechanical Stress, Temperature, and Other Physical Stimuli. Genetics *212*, 25–51.

Goulev, Y., Morlot, S., Matifas, A., Huang, B., Molin, M., Toledano, M.B., and Charvin, G. (2017). Nonlinear feedback drives homeostatic plasticity in H2O2 stress response. Elife *6*.

Gourgou, E., and Chronis, N. (2016). Chemically induced oxidative stress affects ASH neuronal function and behavior in C. elegans. Sci. Rep. *6*, 38147.

Groitl, B., and Jakob, U. (2014). Thiol-based redox switches. Biochim. Biophys. Acta *1844*, 1335–1343.

Haes, W.D., De Haes, W., Frooninckx, L., Van Assche, R., Smolders, A., Depuydt, G., Billen, J., Braeckman, B.P., Schoofs, L., and Temmerman, L. (2014). Metformin promotes lifespan through mitohormesis via the peroxiredoxin PRDX-2. Proceedings of the National Academy of Sciences *111*, E2501–E2509.

Hall, A., Karplus, P.A., and Poole, L.B. (2009). Typical 2-Cys peroxiredoxins--structures, mechanisms and functions. FEBS J. *276*, 2469–2477.

Hilliard, M.A., Bargmann, C.I., and Bazzicalupo, P. (2002). C. elegans responds to chemical repellents by integrating sensory inputs from the head and the tail. Curr. Biol. *12*, 730–734.

Hirani, N., Westenberg, M., Gami, M.S., Davis, P., Hope, I.A., and Dolphin, C.T. (2013). A simplified counter-selection recombineering protocol for creating fluorescent protein reporter constructs directly from C. elegans fosmid genomic clones. BMC Biotechnol. *13*, 1.

Ho, B., Baryshnikova, A., and Brown, G.W. (2018). Unification of Protein Abundance Datasets Yields a Quantitative Saccharomyces cerevisiae Proteome. Cell Syst *6*, 192-205.e3.

Isermann, K., Liebau, E., Roeder, T., and Bruchhaus, I. (2004). A peroxiredoxin specifically expressed in two types of pharyngeal neurons is required for normal growth and egg production in Caenorhabditis elegans. J. Mol. Biol. *338*, 745–755.

Jang, H.H., Lee, K.O., Chi, Y.H., Jung, B.G., Park, S.K., Park, J.H., Lee, J.R., Lee, S.S., Moon, J.C., Yun, J.W., et al. (2004). Two Enzymes in One. Cell *117*, 625–635.

Jarvis, R.M., Hughes, S.M., and Ledgerwood, E.C. (2012). Peroxiredoxin 1 functions as a signal peroxidase to receive, transduce, and transmit peroxide signals in mammalian cells. Free Radic. Biol. Med. *53*, 1522–1530.

Jose, A.M., Bany, I.A., Chase, D.L., and Koelle, M.R. (2007). A specific subset of transient receptor potential vanilloid-type channel subunits in Caenorhabditis elegans endocrine cells function as mixed heteromers to promote neurotransmitter release. Genetics *175*, 93–105.

Kamath, R.S., Fraser, A.G., Dong, Y., Poulin, G., Durbin, R., Gotta, M., Kanapin, A., Le Bot, N., Moreno, S., Sohrmann, M., et al. (2003). Systematic functional analysis of the Caenorhabditis elegans genome using RNAi. Nature *421*, 231–237.

Kim, K., and Li, C. (2004). Expression and regulation of an FMRFamide-related neuropeptide gene family in Caenorhabditis elegans. J. Comp. Neurol. *475*, 540–550.

Kopito, R.B., and Levine, E. (2014). Durable spatiotemporal surveillance of Caenorhabditis elegans response to environmental cues. Lab Chip *14*, 764–770.

Kuramochi, M., and Doi, M. (2019). An Excitatory/Inhibitory Switch From Asymmetric Sensory Neurons Defines Postsynaptic Tuning for a Rapid Response to NaCl in Caenorhabditis elegans. Frontiers in Molecular Neuroscience *11*.

Ledgerwood, E.C., Marshall, J.W.A., and Weijman, J.F. (2017). The role of peroxiredoxin 1 in redox sensing and transducing. Arch. Biochem. Biophys. *617*, 60–67.

Lee, J., Godon, C., Lagniel, G., Spector, D., Garin, J., Labarre, J., and Toledano, M.B. (1999). Yap1 and Skn7 control two specialized oxidative stress response regulons in yeast. J. Biol. Chem. *274*, 16040–16046.

Li, G., Gong, J., Lei, H., Liu, J., and Shawn Xu, X.Z. (2016). Promotion of behavior and neuronal function by reactive oxygen species in C. elegans. Nature Communications *7*.

Liu, J., Ward, A., Gao, J., Dong, Y., Nishio, N., Inada, H., Kang, L., Yu, Y., Ma, D., Xu, T., et al. (2010). C. elegans phototransduction requires a G protein–dependent cGMP pathway and a taste receptor homolog. Nature Neuroscience *13*, 715–722.

Lorenzo, R., Onizuka, M., Defrance, M., and Laurent, P. (2020). Combining single-cell RNA-sequencing with a molecular atlas unveils new markers for Caenorhabditis elegans neuron classes. Nucleic Acids Res. *48*, 7119–7134.

Low, F.M., Hampton, M.B., Peskin, A.V., and Winterbourn, C.C. (2007). Peroxiredoxin 2 functions as a noncatalytic scavenger of low-level hydrogen peroxide in the erythrocyte. Blood *109*, 2611–2617.

McCallum, K.C., Liu, B., Fierro-González, J.C., Swoboda, P., Arur, S., Miranda-Vizuete, A., and Garsin, D.A. (2016). TRX-1 Regulates SKN-1 Nuclear Localization Cell Non-autonomously in Caenorhabditis elegans. Genetics *203*, 387–402.

Miranda-Vizuete, A., González, J.C.F., Gahmon, G., Burghoorn, J., Navas, P., and Swoboda, P. (2006). Lifespan decrease in aCaenorhabditis elegansmutant lacking TRX-1, a thioredoxin expressed in ASJ sensory neurons. FEBS Letters *580*, 484–490.

Mizuno, T., Hisamoto, N., Terada, T., Kondo, T., Adachi, M., Nishida, E., Kim, D.H., Ausubel, F.M., and Matsumoto, K. (2004). The Caenorhabditis elegans MAPK phosphatase VHP-1 mediates a novel JNK-like signaling pathway in stress response. EMBO J. *23*, 2226–2234.

Moon, J.C., Hah, Y.S., Kim, W.Y., Jung, B.G., and Jang, H.H. (2005). Oxidative stress-dependent structural and functional switching of a human 2-Cys peroxiredoxin isotype II that enhances HeLa cell resistance to H2O2-induced cell …. Journal of Biological.

Netto, L.E.S., and Antunes, F. (2016). The Roles of Peroxiredoxin and Thioredoxin in Hydrogen Peroxide Sensing and in Signal Transduction. Mol. Cells *39*, 65–71.

Niu, W., Lu, Z.J., Zhong, M., Sarov, M., Murray, J.I., Brdlik, C.M., Janette, J., Chen, C., Alves, P., Preston, E., et al. (2011). Diverse transcription factor binding features revealed by genome-wide ChIP-seq in C. elegans. Genome Res. *21*, 245–254.

Ohnishi, K., Saito, S., Miura, T., Ohta, A., Tominaga, M., Sokabe, T., and Kuhara, A. (2020). OSM-9 and OCR-2 TRPV channels are accessorial warm receptors in Caenorhabditis elegans temperature acclimatisation. Sci. Rep. *10*, 18566.

Oláhová, M., Taylor, S.R., Khazaipoul, S., Wang, J., Morgan, B.A., Matsumoto, K., Blackwell, T.K., and Veal, E.A. (2008). A redox-sensitive peroxiredoxin that is important for longevity has tissue- and stress-specific roles in stress resistance. Proc. Natl. Acad. Sci. U. S. A. *105*, 19839–19844.

Park, M.H., Jo, M., Kim, Y.R., Lee, C.-K., and Hong, J.T. (2016). Roles of peroxiredoxins in cancer, neurodegenerative diseases and inflammatory diseases. Pharmacology & Therapeutics *163*, 1–23.

Randall, L.M., Ferrer-Sueta, G., and Denicola, A. (2013). Peroxiredoxins as preferential targets in H2O2-induced signaling. Methods Enzymol. *527*, 41–63.

Rangaraju, S., Solis, G.M., Andersson, S.I., Gomez-Amaro, R.L., Kardakaris, R., Broaddus, C.D., Niculescu, A.B., 3rd, and Petrascheck, M. (2015). Atypical antidepressants extend lifespan of Caenorhabditis elegans by activation of a non-cell-autonomous stress response. Aging Cell *14*, 971–981.

Rhee, S.G., and Woo, H.A. (2011). Multiple Functions of Peroxiredoxins: Peroxidases, Sensors and Regulators of the Intracellular Messenger H2O2, and Protein Chaperones. Antioxid. Redox Signal. *15*, 781–794.

Sanzo-Machuca, Á., Monje Moreno, J.M., Casado-Navarro, R., Karakuzu, O., Guerrero-Gómez, D., Fierro-González, J.C., Swoboda, P., Muñoz, M.J., Garsin, D.A., Pedrajas, J.R., et al. (2019). Redox-dependent and redox-independent functions of Caenorhabditis elegans thioredoxin 1. Redox Biol *24*, 101178.

Schwartz, M.L., and Jorgensen, E.M. (2016). SapTrap, a Toolkit for High-Throughput CRISPR/Cas9 Gene Modification in Caenorhabditis elegans. Genetics *202*, 1277–1288.

Stöcker, S., Maurer, M., Ruppert, T., and Dick, T.P. (2018). A role for 2-Cys peroxiredoxins in facilitating cytosolic protein thiol oxidation. Nat. Chem. Biol. *14*, 148–155.

Tang, L., Dodd, W., and Choe, K. (2016). Isolation of a Hypomorphic skn-1 Allele That Does Not Require a Balancer for Maintenance. G3 Genes|Genomes|Genetics *6*, 551–558.

Thamsen, M., Kumsta, C., Li, F., and Jakob, U. (2011). Is Overoxidation of Peroxiredoxin Physiologically Significant? Antioxidants & Redox Signaling *14*, 725–730.

Tian, L., Hires, S.A., Mao, T., Huber, D., Chiappe, M.E., Chalasani, S.H., Petreanu, L., Akerboom, J., McKinney, S.A., Schreiter, E.R., et al. (2009). Imaging neural activity in worms, flies and mice with improved GCaMP calcium indicators. Nat. Methods *6*, 875–881.

Veal, E.A., Day, A.M., and Morgan, B.A. (2007). Hydrogen peroxide sensing and signaling. Mol. Cell *26*, 1–14.

Ward, A., Liu, J., Feng, Z., and Shawn Xu, X.Z. (2008). Light-sensitive neurons and channels mediate phototaxis in C. elegans. Nature Neuroscience *11*, 916–922.

Winterbourn, C.C., and Peskin, A.V. (2016). Kinetic Approaches to Measuring Peroxiredoxin Reactivity. Mol. Cells *39*, 26–30.

Wu, F., Chi, Y., Jiang, Z., Xu, Y., Xie, L., Huang, F., Wan, D., Ni, J., Yuan, F., Wu, X., et al. (2020). Hydrogen peroxide sensor HPCA1 is an LRR receptor kinase in Arabidopsis. Nature *578*, 577–581.

Yan, Y., Sabharwal, P., Rao, M., and Sockanathan, S. (2009). The antioxidant enzyme Prdx1 controls neuronal differentiation by thiol-redox-dependent activation of GDE2. Cell *138*, 1209–1221.

Yemini, E., Lin, A., Nejatbakhsh, A., Varol, E., Sun, R., Mena, G.E., Samuel, A.D.T., Paninski, L., Venkatachalam, V., and Hobert, O. (2021). NeuroPAL: A Multicolor Atlas for Whole-Brain Neuronal Identification in C. elegans. Cell *184*, 272-288.e11.

Zhang, W., He, F., Ronan, E.A., Liu, H., Gong, J., Liu, J., and Xu, X.Z.S. (2020). Regulation of photosensation by hydrogen peroxide and antioxidants in C. elegans. PLoS Genet. *16*, e1009257.

Zou, W., Cheng, H., Li, S., Yue, X., Xue, Y., Chen, S., and Kang, L. (2017). Polymodal Responses in C. elegans Phasmid Neurons Rely on Multiple Intracellular and Intercellular Signaling Pathways. Sci. Rep. *7*, 42295.

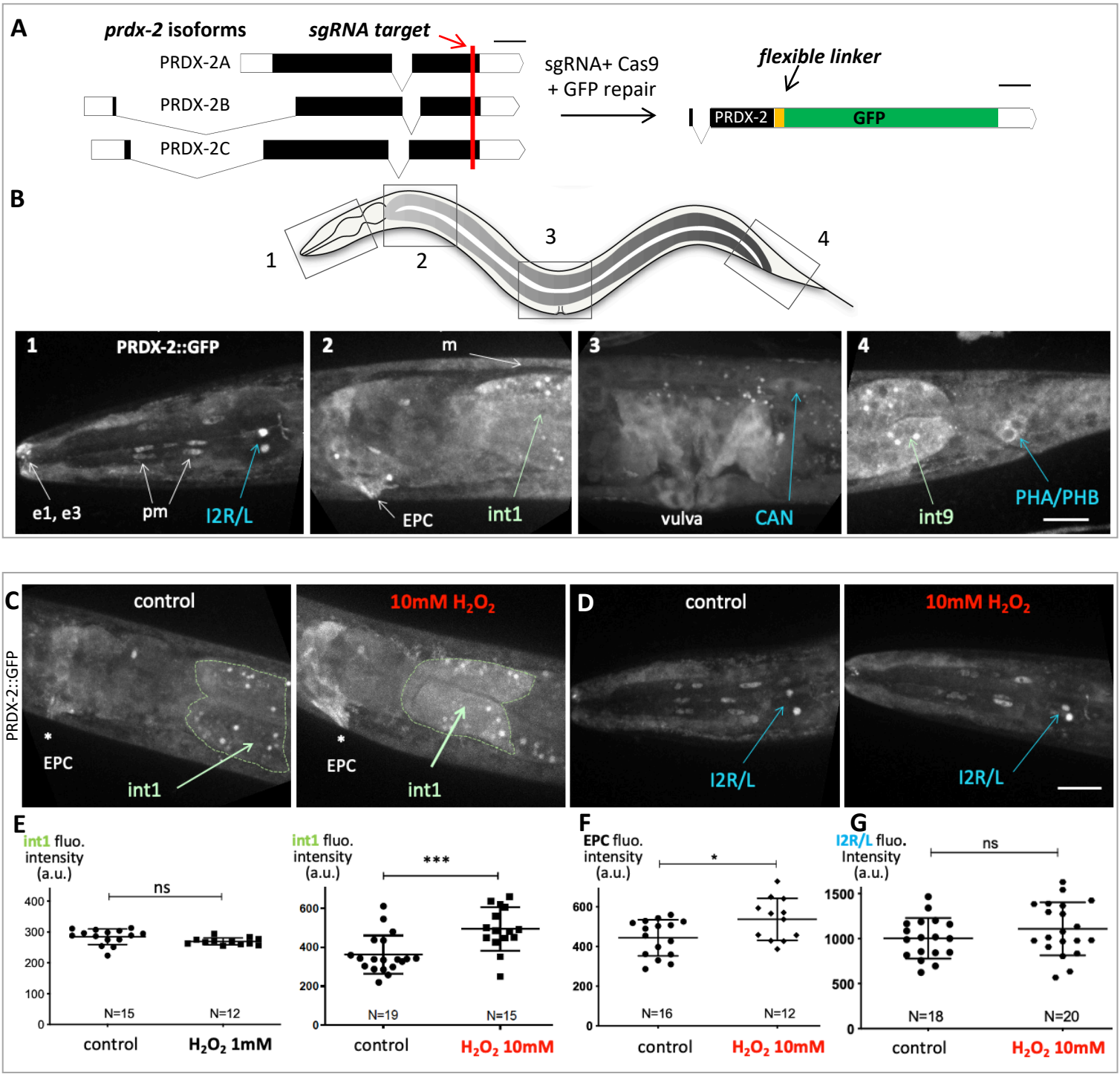
A
prdx-2 isoforms
sgRNA target
PRDX-2A
PRDX-2B
PRDX-2C
sgRNA+ Cas9
+ GFP repair
flexible linker
PRDX-2
GFP
B
1
2
3
4
PRDX-2::GFP
m
e1, e3
pm
I2R/L
EPC
int1
vulva
CAN
int9
PHA/PHB
C
control
10mM H2O2
PRDX-2::GFP
EPC
int1
D
I2R/L
E
int1 fluo. intensity (a.u.)
ns
N=15
N=12
control
H2O2 1mM
***
N=19
N=15
H2O2 10mM
F
EPC fluo. intensity (a.u.)
*
N=16
N=12
G
I2R/L fluo. Intensity (a.u.)
N=18
N=20

Figure 1

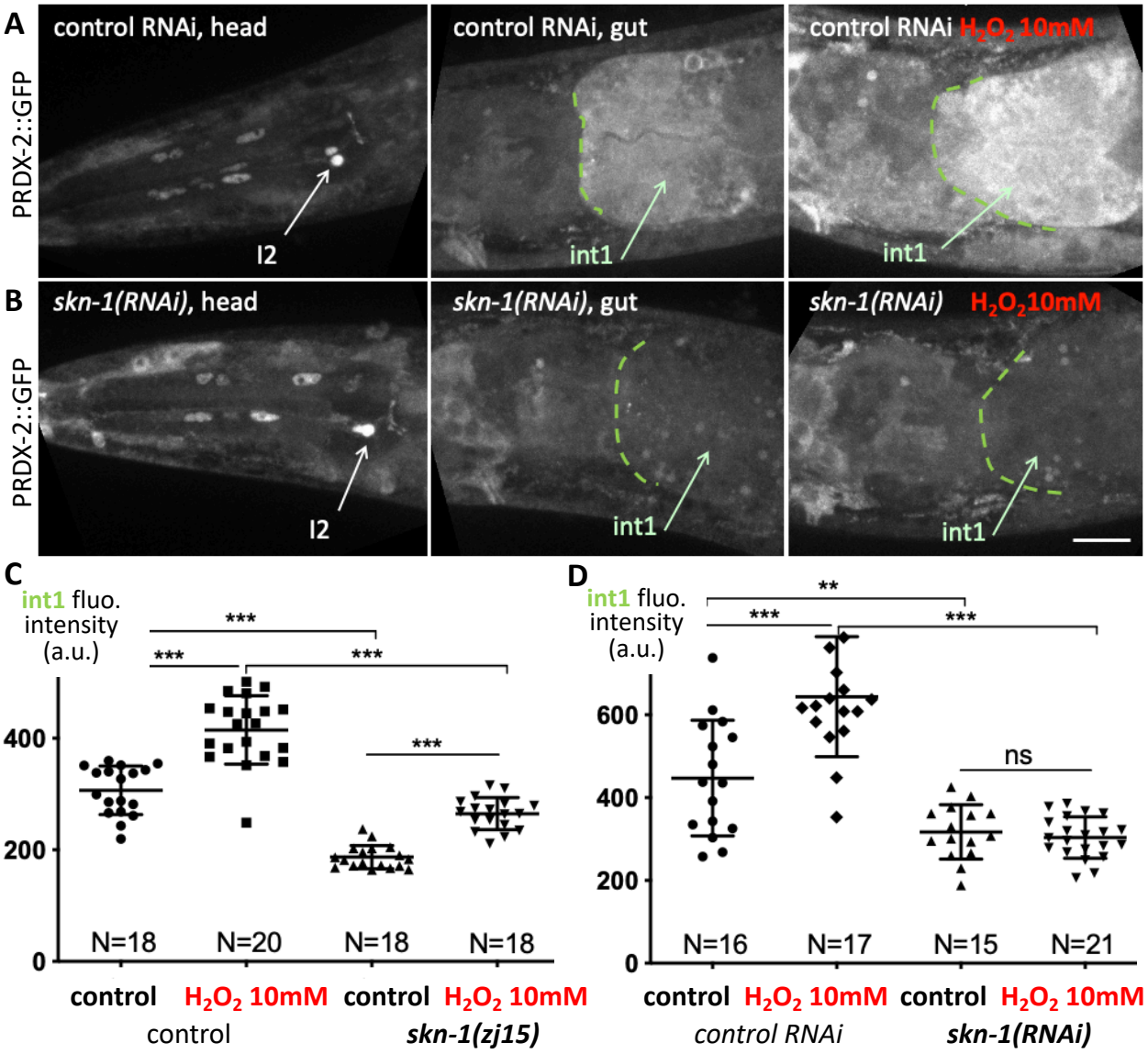

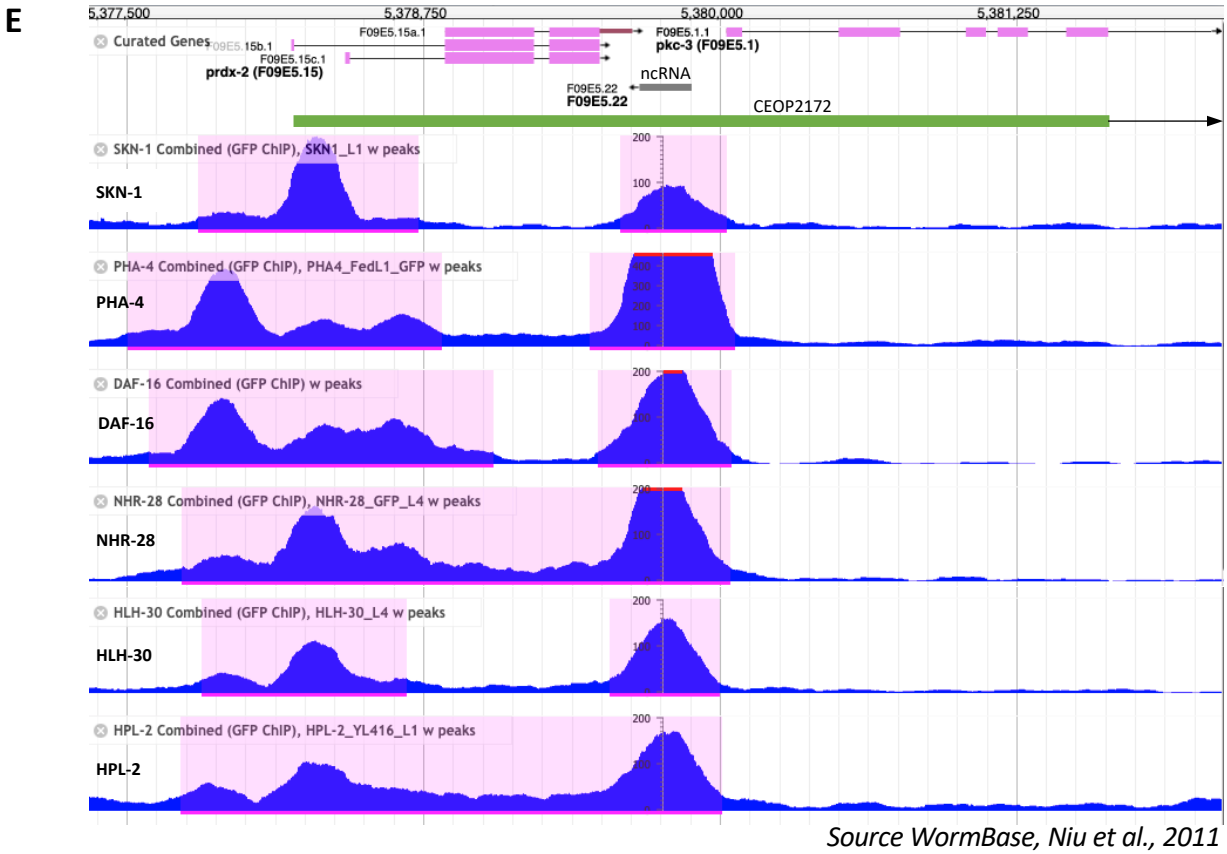

Source WormBase, Niu et al., 2011

Figure 2

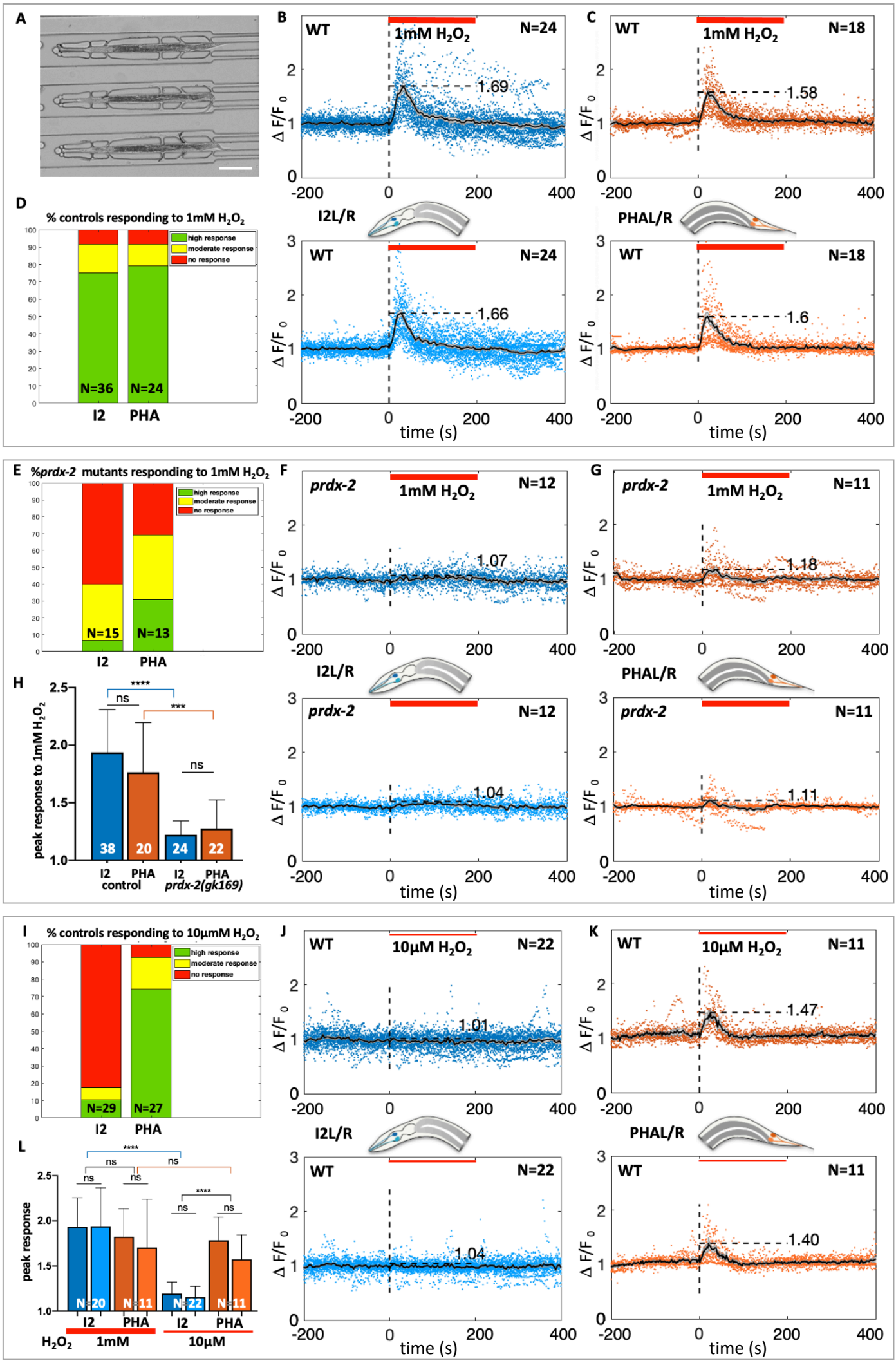
A
B
WT
1mM H_2O_2
N=24
1.69
C
WT
1mM H_2O_2
N=18
1.58
D
% controls responding to 1mM H_2O_2
high response
moderate response
no response
N=36
N=24
I2
PHA
I2L/R
PHAL/R
WT
N=24
1.66
WT
N=18
1.6
Δ F/F 0
time (s)
E
%prdx-2 mutants responding to 1mM H_2O_2
N=15
N=13
F
prdx-2
1mM H_2O_2
N=12
1.07
G
prdx-2
1mM H_2O_2
N=11
1.18
H
peak response to 1mM H_2O_2
****
ns
***
ns
38
20
24
22
I2
PHA
control
prdx-2(gk169)
prdx-2
N=12
1.04
prdx-2
N=11
1.11
I
% controls responding to 10μmM H_2O_2
N=29
N=27
J
WT
10μM H_2O_2
N=22
1.01
K
WT
10μM H_2O_2
N=11
1.47
L
peak response
N=20
N=11
N=22
N=11
H_2O_2
1mM
10μM
WT
N=22
1.04
WT
N=11
1.40

Figure 3

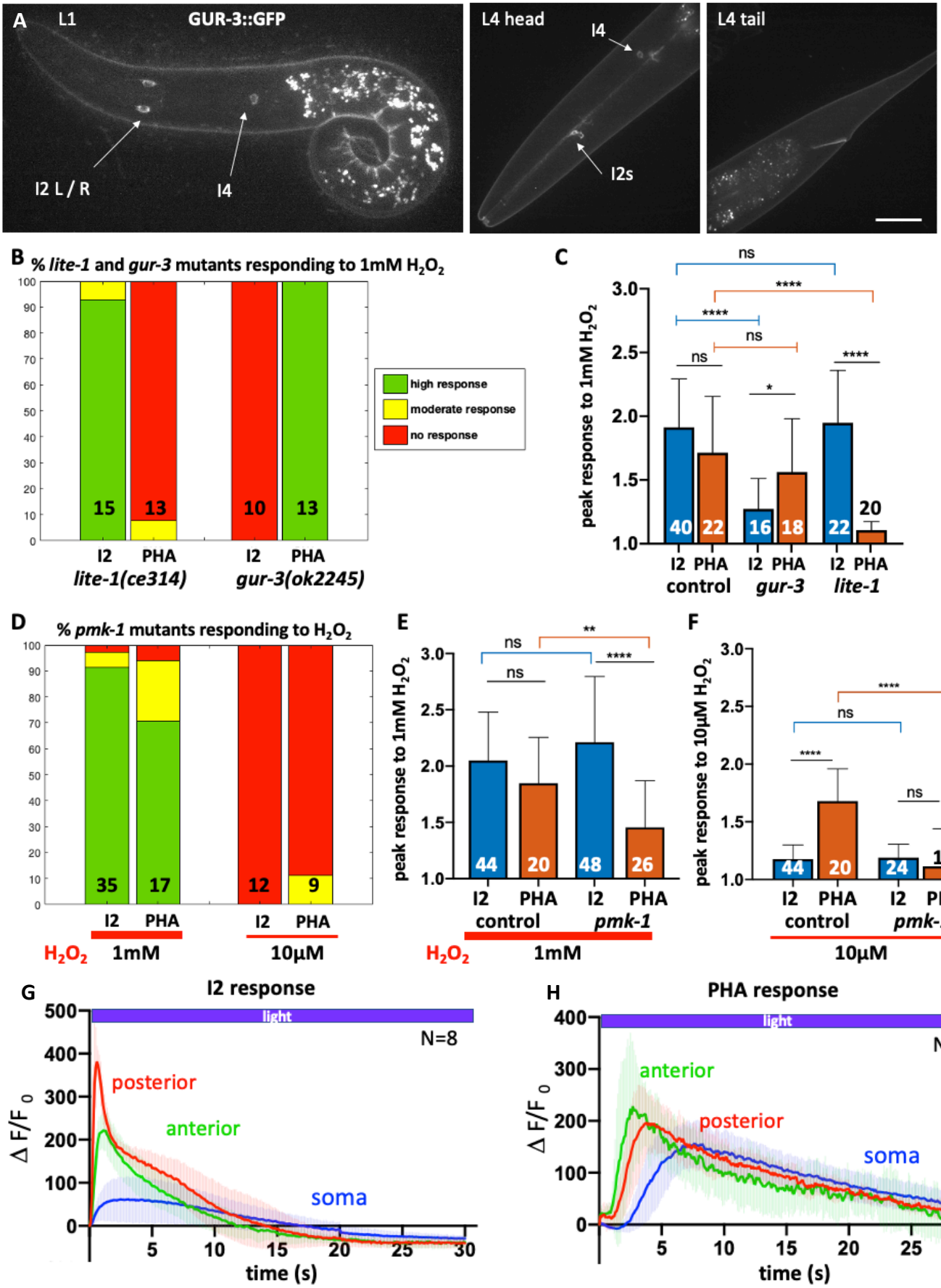
A
L1
GUR-3::GFP
I2 L / R
I4
L4 head
I4
I2s
L4 tail
B
% lite-1 and gur-3 mutants responding to 1mM H2O2
high response
moderate response
no response
15
13
10
13
I2
PHA
I2
PHA
lite-1(ce314)
gur-3(ok2245)
C
peak response to 1mM H2O2
ns
****
****
ns
ns
*
****
40
22
16
18
22
20
I2
PHA
I2
PHA
I2
PHA
control
gur-3
lite-1
D
% pmk-1 mutants responding to H2O2
35
17
12
9
I2
PHA
I2
PHA
H2O2
1mM
10µM
E
peak response to 1mM H2O2
ns
**
ns
****
44
20
48
26
I2
PHA
I2
PHA
control
pmk-1
H2O2
1mM
F
peak response to 10µM H2O2
****
ns
****
ns
44
20
24
18
I2
PHA
I2
PHA
control
pmk-1
10µM
G
I2 response
light
N=8
posterior
anterior
soma
Δ F/F 0
time (s)
H
PHA response
light
N=7
anterior
posterior
soma
Δ F/F 0
time (s)

Figure 4

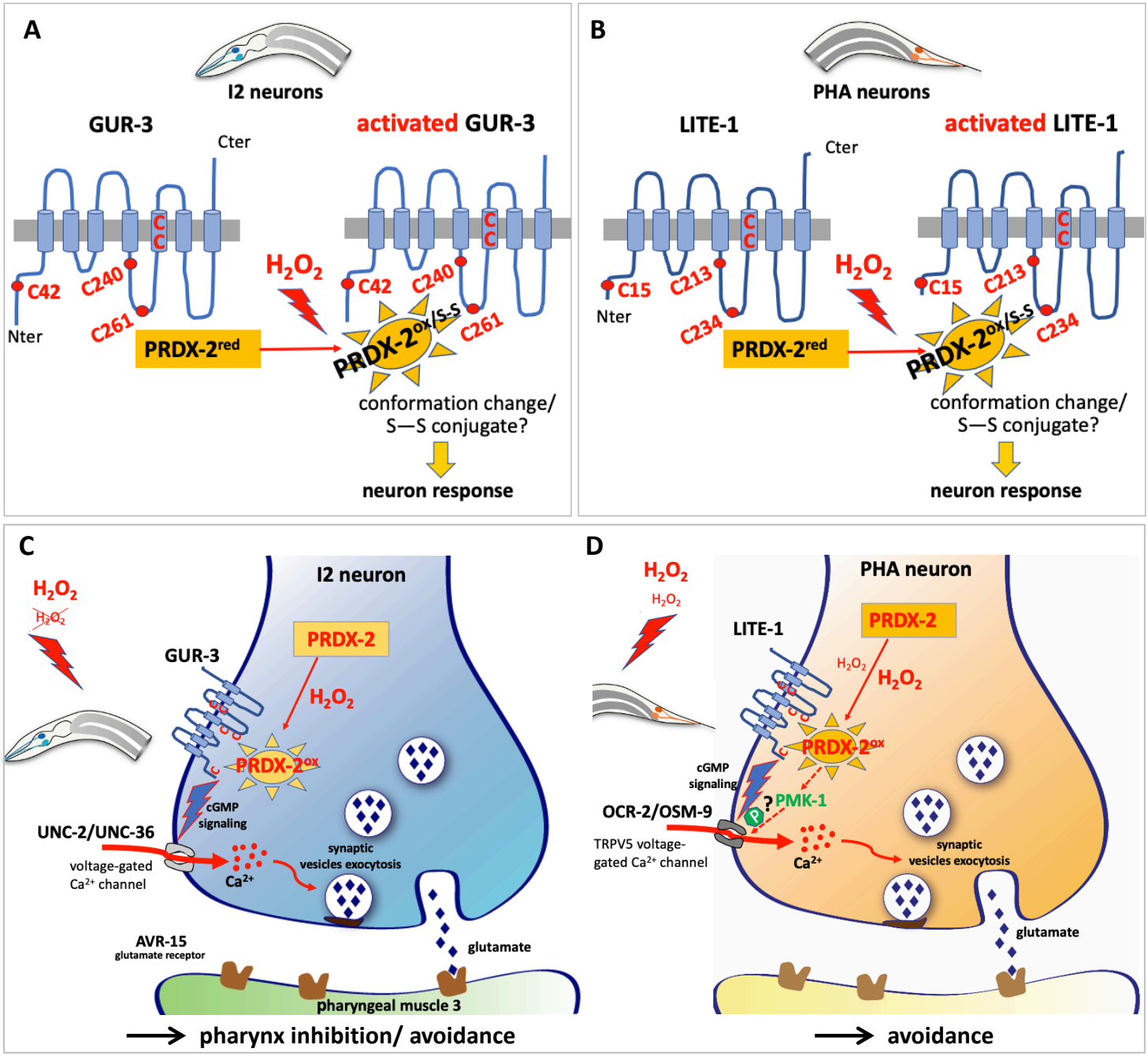
A
I2 neurons
GUR-3
activated GUR-3
Cter
C42
C240
C261
Nter
PRDX-2red
H2O2
PRDX-2ox/S-S
conformation change/
S—S conjugate?
neuron response
B
PHA neurons
LITE-1
activated LITE-1
Cter
C15
C213
C234
Nter
PRDX-2red
H2O2
PRDX-2ox/S-S
conformation change/
S—S conjugate?
neuron response
C
H2O2
I2 neuron
PRDX-2
GUR-3
H2O2
PRDX-2ox
cGMP
signaling
UNC-2/UNC-36
voltage-gated
Ca2+ channel
Ca2+
synaptic
vesicles exocytosis
AVR-15
glutamate receptor
glutamate
pharyngeal muscle 3
pharynx inhibition/ avoidance
D
H2O2
PHA neuron
LITE-1
PRDX-2
H2O2
PRDX-2ox
cGMP
signaling
? PMK-1
OCR-2/OSM-9
TRPV5 voltage-
gated Ca2+ channel
Ca2+
synaptic
vesicles exocytosis
glutamate
avoidance

Figure 5

Figure Legends

Figure 1- PRDX-2::GFP knock-in line expression pattern and its evolution upon H_2O_2 treatment

(A)- Sketch depicting the PRDX-2::GFP knock-in strategy using CRISPR Cas9-mediated genome editing. The sgRNA target sequence (shown in red) was chosen a few base pairs upstream PRDX-2 STOP codon, to tag all *prdx-2* isoforms. Black boxes indicate exons, white boxes unstranslated regions. Bar, 100 bases pairs. The last exon of the PRDX-2::GFP fusion protein is shown on the right; note the insertion of a flexible linker between PRDX-2 and the GFP, likely allowing its correct folding. After injection, three independent knock-in lines were recovered, sharing the same expression pattern. (B) Spinning-disc confocal projections of a representative PRDX-2::GFP knock-in animal, in 4 body regions (correspondingly boxed in the worm drawing). PRDX-2::GFP expression is observed in the tip of the nose (e3 cell), in pharyngeal muscle cells (pm), in body wall muscles (m), in the excretory pore cell (EPC), in proximal and distal gut cells (int1 and int9), and in several neuron pairs, indicated in blue. Note the different level of PRDX-2 between I2 left and right neurons in panel B1. (C-G) An acute oxidative stress triggers an upregulation of PRDX-2 in the foregut, but not in neurons. (C-D) Spinning-disc confocal projections of control or H_2O_2-treated animals in the foregut (C) or in the head region (D). (E-G) Quantification of fluorescence intensity in controls and in H_2O_2-treated animals in the int1 cell (E), in the EPC (F), and I2 neurons (G). Bars indicate mean and s.d. ns, not significant, $p>0.05$; *$p<0.05$; ***$p<0.001$. Scale bar, 20µm.

Figure 2- SKN-1 function is required for PRDX-2 expression in the gut

(A-B)- Spinning-disc confocal projections of head and foregut of PRDX-2::GFP knock-in animals, in control RNAi (A) and in *skn-1(RNAi)* animals (B). The right panel shows the foregut of a 10mM H_2O_2-treated animal in both genotypes. Note the low level of int1 PRDX-2::GFP fluorescence in *skn-1(RNAi)* animal. (C-D) Quantification of the int1 cell fluorescence intensity in control and after a 10mM H_2O_2-treatment, in *skn-1(zj15)* mutants (C) and in *skn-1(RNAi)* animals (D). Bars indicate mean and s.d. ns, not significant, $p>0.05$; **$p<0.01$; ***$p<0.001$. Scale bar, 20µm. (E) Genome Browser from WormBase (release WS283, JBrowse II) showing the peaks detected by ChIP-seq using an anti-GFP antibody (Niu et al., 2011) in *prdx-2* and *pkc-3* promoters, in GFP-tagged transgenic lines of the indicated transcription factors. Top numbers indicate the coordinates on chromosome II. Note the co-regulation of the *prdx-2* and *pkc-3*, which are organized in an operon, indicated by the green bar.

Figure 3- I2 and PHA neurons both respond to 1mM H_2O_2 in a *prdx-2*-dependent manner, but only PHA neurons respond to 10µM H_2O_2

(A)- Low-magnification DIC picture of L4 animals trapped in the microfluidic device used in neuron recordings experiments, as in (B,C,F,G,J,K), which indicate I2R/I2L responses (B,F,J) and PHAL/PHAR responses (C,G,K) to a H_2O_2 stimulation at the dose indicated below the red bar. The average curves show the normalized calcium response measured over time (indicated in seconds) using the GCaMP3 sensor expressed in I2 and PHA neurons, for left and right neurons (top and bottom curves). N, number of movies quantified for each genotype, in wild-type (B,C,J,K) and in *prdx-2* mutants (F,G). (D,E,I) Bar graph of the fraction of animals responding to the H_2O_2 stimulation in all experiments, classified as high (green), moderate (yellow) or absent (red) responses (see Methods). N, number of movies analyzed. (H,L) Quantification of the

calcium response to H_2O_2 in I2 and PHA in controls and *prdx-2* mutants at 1mM (H) and in I2LR and PHALR controls, at 1mM and 10µM (L). The number of movies quantified is indicated on each column. Bars indicate mean and s.d. ns, not significant, p>0.05; ***p<0.001; ****p<0.0001. See also Movies 1-6 and sup. Fig. 5.

Figure 4- The GUR-3 receptor is required in I2 neurons while *lite-1* and *pmk-1* functions are required in PHA response to H_2O_2

(A)- Spinning-disc confocal projections of a representative GUR-3::GFP knock-in animal, at L1 (left) and L4 stages (right). GUR-3::GFP signal is detected in I2 neurons and in a single I4 neurons (head panel), but not in PHA/PHB neurons (tail panel). Bar, 10µm. (B,D) Bar graph of the fraction of *lite-1* and *gur-3* mutants responding to the H_2O_2 stimulation, classified as high (green), moderate (yellow) or absent (red) responses. N, number of movies analyzed. (C,E,F)- Quantification of the calcium response to 1mM H_2O_2 in I2 and PHA neurons in controls and in *gur-3* and *lite-1* mutants (C), and in *pmk-1* mutants at 1mM (E) and 10µM H_2O_2 (F). The number of movies quantified is indicated on each column. Bar, s.d.; ns, not significant, p>0.05; *p<0.05; **p<0.01; ****p<0.0001. See also Movies 7-14 and sup. Figs. 6, 7. (G,H)- Blue light triggered different calcium fluxes in I2 and PHA neurons in the three regions analyzed; anterior neurite (green), posterior neurite (red) and soma (blue). Bars indicate s.d. See Movies 15-17.

Figure 5- Model of H_2O_2 sensing in *C. elegans* via I2 and PHA neurons based on this and previous work

(A-B)- A putative PRDX-2 redox relay may trigger H_2O_2-induced receptor activation. Sketch of GUR-3 (A) and LITE-1 (B) gustatory receptors structure (present in I2 and PHA neurons), showing their 5 conserved cysteins in the intracellular and in the fifth transmembrane domains. In the presence of H_2O_2, oxidized or disulfide form of PRDX-2 (PRDX-$2^{ox/S\text{-}S}$) could oxidize these cysteines, possibly forming a disulfide conjugate and/or inducing a conformation change which triggers receptor activation. (B)- Hypothetic model of of H_2O_2-induced neuronal activation, based on our data and on previous studies. Schematic drawing of a presynaptic button in I2 (C) and PHA (D) neurons, illustrating the presumptive H_2O_2-PRDX-2-mediated neuronal activation in both cases. High doses of H_2O_2 (1mM) are sensed by both neurons, but only PHA responds to 10µM H_2O_2, as indicated in red. In this presumptive model, H_2O_2 would freely diffuse across the neuron plasma membrane and oxidize PRDX-2, presumably leading to LITE-1 or GUR-3 activation. Receptor activation is likely relayed by cGMP signaling, resulting in the opening of voltage-gated calcium channels (depicted in green) and neurotransmitter release (glutamate in both cases), triggering an adapted response. In PHA neurons, PMK-1/p38MAPK activity is additionally required to promote neuronal response to a low dose of H_2O_2, potentially through OSM-9 phosphorylation as observed in ASH neurons (Li et al., 2016). See discussion for further details and bibliographic references.